

# Vehicle Flow Positioning and Real-time Monitoring Based on RFID Vehicle Flow Speeding Automatic Monitoring Algorithm

Yun Bai<sup>1,\*</sup>

<sup>1</sup>Chongqing Industry Polytechnic College, Chongqing, China, 401120

## Article Info

Volume 83

Page Number: 6114 - 6125

Publication Issue:

July - August 2020

## Abstract

Highway traffic safety management is an essential part of the highway operation management system. It plays a vital role in ensuring highway traffic safety and clear roads. In this paper, an accurate real-time positioning and monitoring algorithm based on RFID vehicle flow speeding automatic monitoring. The highway speed measurement system is used to collect the data on the traffic flow and speed of vehicles passing Shanfen highway monitoring point. Through statistical analysis of sample data in the traffic database, the changes in the average speed, speeding volume and rate in this section before and after the enforcement of illegal speeding vehicles were compared and analyzed by the speed measurement system. The positioning and real-time monitoring were completed by extracting the feature information of the visual perception images in the positioning and real-time monitoring range based on the visual perception technology. The inertial information is combined to perform unscented Kalman filtering to improve the accuracy further. Based on the simulation results, the impact of the detection line setting on the detection accuracy is analyzed, the detection and discrimination process of the detection algorithm is described, the theoretical calculation of the maximum detection speed is conducted, and the rapid recovery technology research on the false detection is performed.

**Keywords:** Vehicular Ad-hoc Network (VANET), Positioning and Real-time Monitoring, Road Side Unit (RSU); High-resolution Estimation;

## Article History

Article Received: 25 April 2020

Revised: 29 May 2020

Accepted: 20 June 2020

Publication: 28 August 2020

## 1. Introduction

The rapid popularization of cars in social life has provided convenience to people. However, it has also imposed tremendous pressure on urban transportation, which leads to a series of problems such as frequent traffic accidents, increased energy consumption, aggravated environmental pollution, and road congestion, etc. <sup>[1-2]</sup> In recent years, with the rapid advancement of information technology

(IT), especially mobile communication technology, the Internet of Vehicles (IoV) technology that adopts the vehicular ad-hoc networks (VANETs) as the primary implementation means has offered great opportunities <sup>[3-4]</sup>. For most of VANETs applications, an essential premise for exerting their function is to implement real-time, precise positioning and real-time monitoring of vehicles. Studies have suggested that if vehicles can obtain the location

information of themselves and the surrounding vehicles in a timely manner and issue an advance warning to the driver before traffic congestion or possible collision occurs, it can reduce traffic accidents by about 40% [5-6].

Precise and real-time vehicle positioning and real-time monitoring technology is a necessary means for safety evaluation and system intervention in the driver assistance system. In addition, it is also the key core technology to the breakthrough for the era of automatic RFID vehicle flow speeding monitoring and accelerated RFID vehicle flow speeding monitoring [7-8]. At present, the research and development of automatic monitoring of automobile RFID traffic flow speeding mainly follow the technical routes of single vehicle intelligence (that is, the so-called "fat system") and intelligent connected vehicle system (that is, the so-called "thin system"). In the aspect of vehicle environmental perception and driving decision, the former is mainly implemented through on-board sensors and processing units; while the latter is mainly implemented through a dedicated wireless network or a public mobile communication network, such as the 5<sup>th</sup> generation (5G) wireless communication system. No matter it is a fat system or a thin system, precise and real-time vehicle positioning and real-time monitoring are essential. For this purpose, many studies have been conducted [9-10]. In this paper, a 3D positioning and real-time monitoring scheme combining perception for RFID vehicle flow speeding automatic monitoring scenes, where three-dimensional candidate frames are generated from the 3D point cloud, and the features from multiple views by area are combined to accomplish the positioning and real-time monitoring. The information from multiple sensors is analyzed and integrated, and the communication network is used to assist in the hierarchical decision-making for the automatic monitoring of RFID vehicle flow speeding. In the BJUT-IV smart car project, a tracking algorithm is used to implement the positioning and real-time monitoring of RFID

vehicle flow speeding automatic monitoring lateral movement. In the algorithm, the preview distance is designed as a function of vehicle parameters and vehicle speed, and the target position is further determined based on the distance. Internet companies such as Google, Uber, and Baidu are also carrying out research on automatic monitoring of vehicles based on the RFID vehicle flow speeding through vehicle sensors. Short-term progress can be achieved based on the single vehicle intelligent mode in urban scenes with relatively complete transportation facilities or highway scenes with relatively simple driving conditions. However, the hardware cost is excessively high, and there are relatively high limitations relying solely on single vehicle intelligence. For example, for complex scenes such as severely damaged facilities, irregularly deployed roads and highways with high traffic flow, or in extreme weather conditions such as rain, snow, and fog that can affect the performance of image sensors and radar, it is highly challenging to complete the road environment perception and real-time decision-making based on single vehicle intelligence. Hence, in order to truly enter the RFID vehicle flow speeding automatic monitoring stage, in addition to the own sensors of vehicles (including millimeter-wave radar, lidar, ultrasonic, camera, and so on), the significance of VANETs is highlighted. VANETs can provide continuous and reliable additional information (such as the ranging information, road conditions, traffic signals, etc.) during the driving process of the vehicles, thereby helping the vehicles determine their position more precisely, and implementing precise positioning and real-time monitoring at the lane level (at the centimeter level). With the research and development of the single vehicle RFID vehicle flow speeding automatic monitoring technology, the research on the application of the Global Navigation Satellite System (GNSS) to vehicle positioning and real-time monitoring is in full swing. However, when a vehicle is driving in densely packed urban streets, overpasses, or tunnels, the GNSS signal of

the vehicle can be easily blocked. As a result, it may not be possible to implement precise and reliable real-time positioning and real-time monitoring, which can severely restrict the application of IoV in urban transportation systems. Hence, in the context of complex urban environments, under the circumstances that the GNSS and other systems fail to provide reliable positioning services for vehicles, the studies of the high-accuracy vehicle real-time positioning and real-time monitoring method based on the VANETs that has strong environmental adaptability and can meet the requirements of most IoV applications are required urgently.

In this paper, a precise, real-time vehicle positioning and real-time monitoring algorithm based on the Matrix Pencil and Non-Linear Fitting (MP-NLF) and visual perception technology is put forward. The algorithm adopts the Road Side Unit (RSU) in the VANETs as a reference node for the wireless positioning and real-time monitoring of vehicles and uses the single RSU to solve the real-time, precise vehicle positioning and real-time monitoring issues effectively, which includes the following: (1) Based on the RFID technology, the frequency domain 1-dimensional MP algorithm is first used to obtain the estimated real-time angle of arrival (AOA). Subsequently, the frequency diversity features of the orthogonal frequency division multiplexing (OFDM) subcarriers are used to establish the model for the high-resolution estimation of time of arrival (TOA) as an NLF problem for solution. In addition, the features of the adjacent subcarrier phase difference are used to improve the estimation performance. Finally, the estimated value for TOA/AOA is input into the weighted least squares (WLS) estimator to implement high-precision real-time positioning and real-time monitoring. (2) Based on the visual perception technology, the image feature information is extracted by configuring a visual sensor at the RSU end to obtain the target vehicle contour and calculate the corresponding centroid coordinates. At the same time, the Unscented Kalman Filter (UKF)

technology is applied to integrate the visual positioning and the real-time monitoring results with the information of the inertial sensor with a relatively high sampling rate further to improve the real-time performance and the positioning and real-time monitoring accuracy. In this paper, the automatic monitoring and assisted driving based on the RFID vehicle flow speeding are studied. A new method and new concept that is different from the current mainstream intelligent RFID vehicle flow speeding automatic monitoring based on the image processing and laser (or millimeter wave) radar are put forward. The simulation results show that, compared with the traditional multi-path fingerprint algorithm, the proposed algorithm has more superior positioning and real-time monitoring performance even in the case of a low signal-to-noise ratio, which can be regarded as an extension of the 5G technology in the direction of automatic monitoring of the RFID vehicle flow speeding. It can solve the problem of the positioning and real-time monitoring at the lane level in IoV applications to a certain extent, which is also of considerable significance to the theoretical research in the field of automatic monitoring of RFID vehicle flow speeding.

## 2. System Model

The scenarios of vehicle positioning and real-time monitoring in this paper are shown in Figure 1. It is assumed that there are typical VANETs distributed on a certain section of the road, and an RSU with a known position is deployed on one side of the road. The RSU can send a beacon packet (BP) containing its own location information to the vehicles within a fixed frequency. Through the IEEE802.11p protocol, the vehicle to infrastructure (V2I) communication can be established between the RSU and the vehicle. It is assumed that the vehicle is equipped with a Uniform Linear Array (ULA) receiver with  $M$  antenna elements (the array direction is orthogonal to the direction of the motion of the vehicle) to receive the BP data transmitted by the RSU and estimate the multi-path TOA and AOA parameters based on the data received. At the same

time, the vehicle is also equipped with an inertial sensor device, which can obtain its own speed information (including the speed amplitude and direction) in real time.

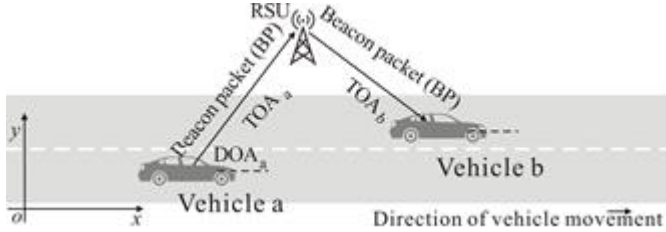


Figure 1. Schematic diagram of vehicle positioning and real-time monitoring scenarios

Figure 2 is the schematic diagram of ULA receiving multi-path signals at the vehicle end. Due to the impact of obstacle reflections, there are P transmission paths between the RSU and the target vehicle. One of the most reliable energy paths is the line of sight (LOS) transmission propagation path (as shown in the solid line), and the remaining paths are non-line of sight. (NLOS) transmission propagation path (as shown in the dashed line). If the preamble of the OFDM frame in the received BP is used to measure the transmission channel information, the least square estimate of the channel frequency response (CFR) on the k-th OFDM subcarrier and the m-th ULA array element can be expressed as the following [13]

$$H_{m,k} = \sum_{p=1}^P \gamma_p e^{-j2\pi f_k(\tau_p + \tau_m(\theta_p))} + w_{m,k} \quad (1)$$

In the above equation,  $\gamma_p$ ,  $\tau_p$  and  $\theta_p$  stand for the transmission gain, propagation delay, and angle of arrival on the p-th path, respectively,  $p = 1, 2, \dots, P$ ;  $e^{-j2\pi f_k(\tau_p + \tau_m(\theta_p))}$  stands for the array response on the m-th antenna array element,  $m = 0, 1, \dots, M - 1$ ;  $\tau_m(\theta_p) = m\tau(\theta_p) = md \sin \theta_p / c$  stands for the difference in the propagation delay of the p-th path between the m-th antenna array element and the reference array element. The parameter d is the distance between adjacent array elements, and c is the propagation speed of the radio wave.  $f_k$  stands

for the carrier frequency of the k-th subcarrier.  $w_{m,k}$  stands for additive white Gaussian noise with a mean of zero and a variance of  $\sigma_w^2 = N_0/2$ . In general, the  $\gamma_p$  of different paths are considered to be independent of each other. However, when the frequency interval between the adjacent subcarriers is greater than the coherent bandwidth, the attenuation between subcarriers is also independent of each other [14]. In this case,  $\gamma_p$  can be replaced by  $\gamma_{k,p}$ . Taking into consideration that in the antenna design, the array element spacing d is usually equal to the half-wavelength of the incident signal, then  $d = c/(2f_c)$  can be obtained. Hence,  $e^{-j2\pi f_c m \tau(\theta_p)}$  can be simplified to  $e^{-jm\pi \sin \theta_p}$ . At the same time, as the antenna element spacing is much smaller than the length of the propagation path, the effect of the propagation delay between the elements on the CFR is much smaller than the effect of the path propagation delay on CFR. Hence, the estimation of CFR at the receiving end can be further simplified to the following

$$H_{m,k} = \sum_{p=1}^P \gamma_{k,p} e^{-j2\pi f_k \tau_p} e^{-j2\pi f_c m \tau(\theta_p)} + w_{m,k} \quad (2)$$

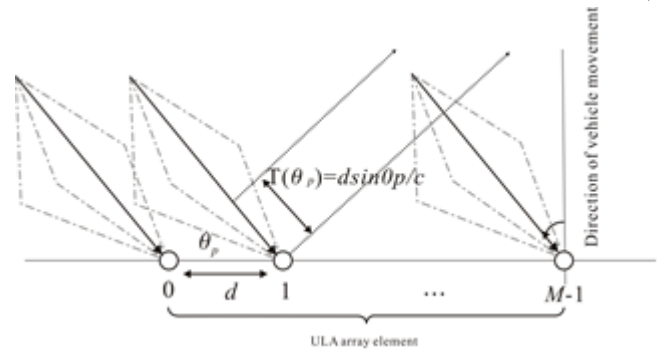


Figure 2. Schematic diagram of ULA receiving multi-path signals at the vehicle end

### 3. Precise Real-time Vehicle Positioning and Real-time Monitoring Algorithm

In this section, the precise, real-time positioning and real-time monitoring algorithms based on the RFID vehicle flow speeding automatic monitoring is provided in detail, including the positioning and real-time monitoring algorithm

based on the RFID technology, as well as the positioning and real-time monitoring algorithm based on visual perception.

### 3.1. Positioning and Real-time Monitoring Algorithm Based on RFID Technology

#### 3.1.1. Application of MP Algorithm for AOA Estimation

In order to apply high-resolution estimation, the CFR estimation matrix expression (2) measured at the receiving end is first described as  $X = [x_0, x_1, \dots, x_{K-1}]$ , and the k-th column of the matrix is expressed as  $x_k = [H_{0,k}, H_{1,k}, \dots, H_{M-1,k}]^T$ , which can be written in the form of vector as the following

$$x_k = Va_k + w_k \quad (3)$$

Different from the traditional high-resolution algorithm that processes multiple sets of snapshot data in the time domain, only a single moment of sampling needs to be used to establish a sampling covariance matrix in the frequency domain, which has greatly reduced the time overhead of the algorithm. The sampling covariance matrix  $R_{xx}$  can be expressed as the following

$$R_{xx} = \frac{1}{K} XX^* = \frac{1}{K} \sum_{k=0}^{K-1} x_k x_k^* \quad (4)$$

Eigenvalue decomposition is carried out on  $R_{xx}$ , and the following can be obtained

$$R_{xx} = \sum_{i=1}^{M-1} \lambda_i u_i u_i^* = U_s \Sigma_s U_s^* + U_n \Sigma_n U_n^* \quad (5)$$

In the above equation,  $\Sigma_s = \text{diag}(\lambda_0, \lambda_1, \dots, \lambda_{p-1})$  stand for P eigenvalues that are relatively large in  $R_{xx}$ , and the remaining eigenvalues are represented by  $\Sigma_n = \text{diag}(\lambda_p, \lambda_{p+1}, \dots, \lambda_{M-1})$ .

$U_s = [u_0, u_1, \dots, u_{p-1}]$  stands for the matrix composed of eigenvectors corresponding to P eigenvalues that are relatively large in  $\Sigma_s$ , which form the signal subspace of the matrix  $R_{xx}$ . The subspace dimension

P can be provided by some estimation algorithms based on the information theory criteria.  $U_n = [u_p, u_{p+1}, \dots, u_{M-1}]$  is a matrix composed of eigenvectors corresponding to the other  $M - P$  eigenvalues, which have formed a noise subspace. Let  $U_1$  and  $U_2$  be the matrix obtained by deleting the last row and the first row of the elements in  $U(n)$ . Hence, the matrix pencil in the spatial dimension can be expressed as  $U_2 - \xi U_1$ , and the multi-path AOA information can be extracted by the generalized eigenvalue decomposition of the matrix  $\psi = U_1^+ U_2$ , as shown in equation (6) below

$$(U_1^+ U_2 - \xi_p I) \varphi_p = 0 \quad (6)$$

In the above equation,  $\varphi_p$  stands for the eigenvector in the  $(U_1^+ U_2 - \xi_p I)$  zero space, and the corresponding eigenvalue is  $\xi_p = e^{-j\pi \sin \theta_p}$ . Hence, the multi-path AOA can be estimated as the following

$$\theta_p = \arcsin \left( \frac{\arg(\xi_p)}{\pi} \right), p = 1, 2, \dots, P \quad (7)$$

In the above equation,  $\arg(\cdot)$  stands for the operation of calculating the phase angle.

#### 3.1.2. Application of NLF for TOA Estimation

After the AOA estimate is obtained, the CFR matrix is transformed into a frequency domain path information matrix  $\Gamma = [a_0, a_1, \dots, a_{K-1}]$ , so that the low-complexity and high-resolution TOA estimation can be implemented through frequency diversity characteristics and NLF technology. In the previous section, the estimate for the multi-path pole  $\xi_p$  has been obtained. After the noise term is ignored, the k-th column of CFR can be written as the following

$$x_k = Ba_k = \begin{bmatrix} \xi_1 & \xi_2 & \dots & \xi_p \\ \xi_1^2 & \xi_2^2 & \dots & \xi_p^2 \\ \vdots & \vdots & \ddots & \vdots \\ \xi_1^M & \xi_2^M & \dots & \xi_p^M \end{bmatrix} \begin{bmatrix} \gamma_{k,1} e^{-j2\pi f_k \tau_1} \\ \gamma_{k,2} e^{-j2\pi f_k \tau_2} \\ \dots \\ \gamma_{k,p} e^{-j2\pi f_k \tau_p} \end{bmatrix} \quad (8)$$

Equation (8) can be derived from Equation (3). In Equation (8), the path vector  $a_k = [\alpha_{k,1}, \alpha_{k,2}, \dots, \alpha_{k,P}]^T$  can be estimated through the complex least squares solution, in which  $\alpha_{k,p} = \gamma_{k,p} e^{-j2\pi f_k \tau_p}$ , as shown in Equation (9) below

$$a_k = (B^* B)^{-1} B^* x_k \quad (9)$$

In the above equation, each element of  $a_k$  contains complex path fading component  $\gamma_{k,p}$  and phase component  $e^{-j2\pi f_k \tau_p}$ . In order to describe the CFR fading characteristics of OFDM signals, the path fading expression based on the Friis formula is rewritten as  $\gamma_{k,p} = \rho_p (4\pi f_k \tau_p)^{-1}$ , in which  $\rho_p$  stands for the environmental factor of the p-th path. Hence, the element  $\alpha_{k,p}$  in  $a_k$  corresponding to the p-th path and the k-th subcarrier can be expressed as the following

$$\alpha_{k,p} = \rho_p (4\pi f_k \tau_p)^{-1} e^{-j2\pi f_k \tau_p} \quad (10)$$

In the above equation,  $\rho_p$  and  $\tau_p$  are both unknown parameters to be estimated. As the fading characteristics of various subcarriers are different, assuming  $K \geq 2P$ , it can be found that the joint estimation issue of parameters  $\rho_p$  and  $\tau_p$  in equation (10) is overdetermined. Hence, the frequency diversity features of the received data can be used to estimate the multi-path TOA information. The  $\alpha_{k,p}$  is fitted with the estimated parameters in equation (9) based on the least squares method. In this way, TOA estimation can be modeled as an NLF problem, and its objective function is defined as the following

$$\min_q F(q) = \sum_{k=0}^{K-1} \mu_k(q) \quad (11)$$

In the above equation,  $q = (\rho_1, \dots, \rho_P, \tau_1, \dots, \tau_P) \in \mathbb{R}^{2P}$  is the set of unknown

parameters, in which  $\mu_k(q)$  stands for the independent fitting error on each sub-carrier, and the expression is as the following

$$\begin{aligned} \mu_k(q) &= \sum_{p=1}^P \left| \alpha_{k,p} - \alpha_{k,p} \right|^2 \\ &= \sum_{p=1}^P \left( \gamma_{k,p}^2 + \left| \alpha_{k,p} \right|^2 - 2\alpha_{k,p} \left( \text{Re}(\alpha_{k,p}) \cos b_{k,p} - \text{Im}(\alpha_{k,p}) \sin b_{k,p} \right) \right) \end{aligned} \quad (12)$$

In the above equation,  $b_{k,p} = 2\pi f_k \tau_p$ ,  $p = 1, 2, \dots, P$ . Through solving the fitting function, the required multi-path TOA estimated value  $\hat{\tau}_p$  can be obtained.

In equation (12), due to the presence of trigonometric functions, the current fitting function cannot identify a precise solution properly. The reason is that in the fitting function,  $\rho_p \tau_p^{-1}$  is the dominant part, which can lead to the ill-conditioned features of the function, that is, even a minor change in the input will cause a relatively huge change in the solution. In order to solve the above problem, the phase difference between the path information of adjacent subcarriers is used as the input of the fitting function to ensure that the input phase of  $\alpha_{k,p}$  is consistent with the phase of  $\alpha_{k,p}$ . Hence, equation (12) can be modified to the following

$$\mu_k(d) = \sum_{p=1}^P \left( 2\pi(f_{k+1} - f_k)\tau_p - \left( \arg(\alpha_{k,p}) - \arg(\alpha_{k,p}) \right) \right)^2 \quad (13)$$

In the above equation,  $d = (\tau_1, \tau_2, \dots, \tau_P) \in \mathbb{R}^P$  is an unknown vector containing the required TOA parameters. The objective function of the fitting problem is rewritten as  $F(d) = \sum_{k=0}^{K-2} \mu_k(d)$ . At this point, the overdetermination condition is also changed into  $K \geq P + 1$ . In urban scenes, the number of multi-paths is generally less than the number of OFDM subcarriers. Hence, this assumption is valid in most cases. In the new objective function, the path fading and trigonometric function parts are removed from the original objective function. As a result, the fitting performance is better, and the volume of

computation is significantly reduced. In addition, the condition number of the Hesse matrix of the new objective function is 1, which is sufficiently small, suggesting that the objective function is no longer ill-conditioned. In the end, the output  $d^*$  of NLF is the estimate of multi-path TOA information, and the TOA estimate  $d$  of the LOS path required for positioning and real-time monitoring is the minimum value in  $d^*$ .

### 3.1.3. Estimation of WLS Position

After the TOA and AOA estimated values of the LOS path are obtained, let  $p_R = [x_R, y_R]^T$  stand for the known position vector of the RSU, as shown in Figure 3. The current position vector  $p = [x, y]^T$  of the vehicle can be expressed as the following

$$p = p_R + \begin{bmatrix} d \cos \theta \\ d \sin \theta \end{bmatrix} \quad (14)$$

In the above equation,  $\theta = (\theta + \dot{\theta}) \% (2\pi)$  stands for the angle between the incident wave and the positive direction of the x-axis, and % indicates the modulus calculation.  $\theta$  and  $\dot{\theta}$  stand for the estimated value of AOA and the heading angle of vehicle movement, respectively. Let  $[v_x, v_y]^T$  represent the speed vector of the vehicle, then the heading angle can be described as  $\dot{\theta} = \arctan(v_y/v_x)$ . As the position information calculated based on equation (14) is affected by channel noise and estimation error, its accuracy cannot meet the requirements of VANETs security applications in general. Hence, in order to further improve the positioning and real-time monitoring performance, given the integration of the vehicle motion model and speed information, a WLS estimator is used to process the position estimate obtained by equation (14). Let  $\{t_k | k = 0, 1, \dots\}$  represent the time when the BP sent by the RSU arrives at the ULA of the receiving end of

the target vehicle.  $p(t_0) = [x(t_0), y(t_0)]^T$  and  $p(t_k) = [x(t_k), y(t_k)]^T$  are used to indicate the position of the vehicle at the moment  $t_0$  and  $t_k$ , respectively. At the same time, it is assumed that the speed of the target vehicle remains unchanged in each time interval. Let  $[v_x(t_k), v_y(t_k)]^T$  represent the vehicle speed vector in the time period  $[t_k, t_{k+1})$ , then the kinematic model shown in equation (15) can be obtained

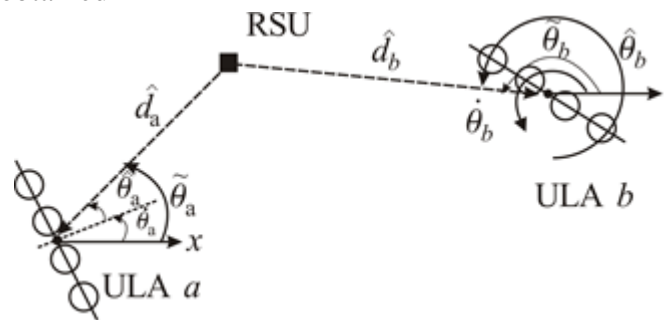


Figure 3. Schematic diagram of ULA receiving at the vehicle end

$$p(t_k) = \begin{bmatrix} x(t_0) + \sum_{j=1}^k v_x(t_{j-1}) \Delta t \\ y(t_0) + \sum_{j=1}^k v_y(t_{j-1}) \Delta t \end{bmatrix} \quad (15)$$

In the above equation,  $\Delta t$  stands for the length of the time interval.

In the calculation of the position of the vehicle at any time, since the speed information is known, and the position vector  $p(t_0)$  at the initial time is unknown, it can be solved through the estimation of equation (16) as the following

$$p(t_0) = \arg \min_{p(t_0)} \sum_{i=1}^k N_i^2 \|p_0(t_i) - p(t_i)\|^2 \quad (16)$$

In the above equation,  $p_0(t_i) = [x_0(t_i), y_0(t_i)]^T$  stands for the rough position estimate obtained by the WLS estimation in step 1 at the moment, and  $p(t_i)$  stands for the position vector calculated based on equation (15).  $N_i$  stands for the SNR measured by the received signal at the moment.

Finally, the unknown vector  $p(t_0)$  can be solved by the least squares method, and the following can be obtained

$$x(t_0) = \frac{\sum_{i=1}^k N_i^2 \left( x_0(t_i) - \sum_{j=1}^i v_x(t_{j-1}) \Delta t \right)}{\sum_{i=1}^k N_i^2} \quad (17)$$

$$y(t_0) = \frac{\sum_{i=1}^k N_i^2 \left( y_0(t_i) - \sum_{j=1}^i v_y(t_{j-1}) \Delta t \right)}{\sum_{i=1}^k N_i^2} \quad (18)$$

### 3.2. Positioning and Real-time Monitoring Algorithm Based on Visual Perception

Visual perception positioning and real-time monitoring are methods where the image processing and the corresponding prior knowledge are used to calculate the position of the vehicle in the environment. As shown in Figure 4, the visual sensor is arranged in the upper part of the RSU in the positioning and real-time monitoring process. The visual perception range of the sensor can cover the road on which the vehicle is running. The positioning and real-time monitoring algorithm based on MP-NLF applies the wireless positioning and real-time monitoring to estimate the single station precise positioning and real-time monitoring of the vehicle through the ranging parameter estimation; while the positioning and real-time monitoring algorithm based on visual perception is a supplement to the algorithm described above. The purpose is to implement effective positioning and real-time monitoring when there are a lot of road obstacles, non-motor vehicles (or pedestrians), or other scenes. The specific steps are described as the following:

Step 1 The real-time images of vehicle operation is obtained through visual sensors arranged on the upper part of RSU;

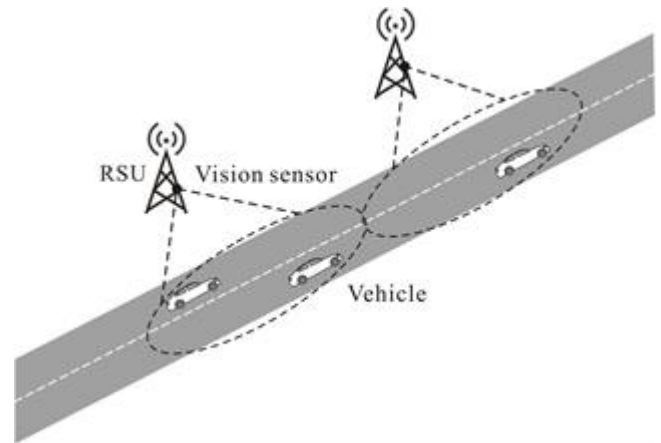


Figure 4. Schematic diagram of vehicle positioning and real-time monitoring based on visual perception

Step 2 For the current frame image within the perception range acquired by the visual sensor, the gray-scale and binary processing is first conducted on the frame image data in sequence. Subsequently, the contour of each object is extracted from the processed image data, and all the contours are filtered to obtain the corresponding contour of the target vehicle. Finally, the centroid coordinates of the vehicle are obtained according to the 2D map information within the perception range constructed based on the frame image. As the centroid coordinates obtained at this time are pixel coordinates, a coordinate conversion operation is required to convert the target vehicle coordinate information in the pixel coordinate system to the motion coordinate system. The coordinate conversion aims first at the image information of the current frame, and the image pixel coordinates  $(u, v)$  are constructed based on the frame image. Subsequently, the image coordinates are converted into the actual motion coordinates  $(x, y)$ . The relationship of the coordinate conversion can be expressed as  $x = au$  and  $y = bu$ . Among them,  $a = \Delta x / W$ ,  $b = \Delta y / H$ ,  $W$  stands for the image width of the current frame in the sensing range,  $H$  stands for the image length of the current frame in the sensing range,  $\Delta x$  stands for the actual ground width of the sensing range, and  $\Delta y$  stands for the actual ground length of the sensing range.

Step 3 According to the current frame image data and the centroid coordinates of each object extracted from the previous frame image data, the contour of each moving object is tracked to prevent the interference of other running objects on the target vehicle. In the tracking process, the distance traveled by each moving object between two frames of images is preset first as a reference value  $D$ . Whenever the sensor acquires the current image within the perception range, for each object contour in the current frame image, the contour with the distance between the previous frame image and the object contour less than  $D$  is regarded as the contour of the moving object. If there is no object contour with a distance less than  $D$  from the contour of the moving object in the previous image, the object contour is regarded as a new moving object that appears in the perception range.

Step 4 Whether the current frame image of the perception range acquired by the visual sensor is the last frame is determined. If it is the last frame, the positioning and real-time monitoring operation ends; if not, return to step 2 when the sensor acquires the next frame image within the perception range and continue the operation. Finally, the RSU sends the vehicle motion coordinates to the vehicle via V2I communication in real time after each frame of image processing is completed.

In the positioning and real-time monitoring process based on visual perception, the images are processed according to each sampling moment to locate and monitor the position of the vehicle in real time, which is susceptible to noise and environmental factors (such as rain, fog, light, and so on). In addition, due to the low scan rate of the visual sensor, it can lead to relatively poor real-time performance of visual positioning and real-time monitoring. Hence, the introduction of UKF technology to combine the visual positioning with real-time monitoring and the own inertial sensor information of the vehicle. It has solved the problem of low real-time performance based on visual positioning and real-time monitoring to a certain

extent and improved the accuracy of positioning and real-time monitoring. UKF is a filtering technique that applies  $\sigma$  points to approximate the nonlinear distribution and reconstruct the parameter system state vectors from the measured values based on the unscented transformation. According to the input data of visual positioning and real-time monitoring system, UKF can effectively integrate the inertial information to filter out any noise interference. At the same time, the relatively high sampling rate of the inertial system can also make up for the problem of poor real-time performance of positioning and real-time monitoring based on visual perception.

#### 4. System Simulation and Discussion

In this section, the performance of the proposed algorithm is analyzed through simulation. The simulation area of vehicle positioning and real-time monitoring is a section of a two-lane straight road with a typical multi-path environment, and the size of the area is  $500\text{m} \times 10\text{m}$ . The RSU used for ranging is deployed at the coordinates (250,15), which can cover the entire positioning and real-time monitoring area. It is assumed that the target vehicle travels along the x-axis in the center line of the second lane, from (0, 2.5) to (500, 2.5), and receives the BP transmitted by RSU through ULA. The simulation scenario is shown in Figure 5 as the following, in which  $p(t_k)$  is the position of the vehicle at the moment  $t_k$ . In order to reflect the dynamic change in the vehicle speed, the driving routes of the vehicle are divided into two paths, which are denoted as  $L_1$  and  $L_2$ , respectively. For the segment  $L_1$ , the vehicle accelerates evenly from 0 km/h to 50 km/h at a constant acceleration. After the vehicle speed reaches 50 km/h, it decelerates uniformly in the segment  $L_2$  until the speed reaches 0 km/h. Through the Monte Carlo simulation, the results of vehicle positioning and real-time monitoring in 1000 driving trajectories are recorded. The specific simulation parameter settings are shown in Table 1 as the following.

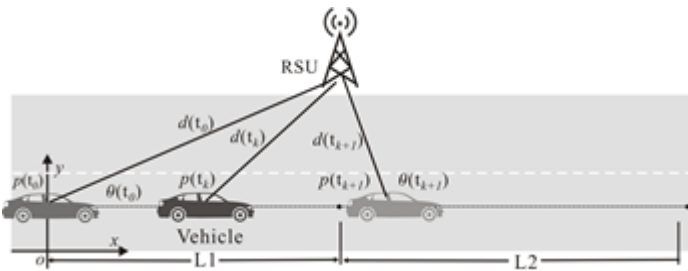


Figure 5. Simulation scene diagram of vehicle positioning and real-time monitoring

A typical urban VANETs positioning and real-time monitoring environment is established according to the simulation parameter settings in Table 1. In this section, the proposed positioning and real-time monitoring algorithm based on RFID technology is used as an example to analyze the positioning and real-time monitoring performance. In order to evaluate the proposed algorithm, the algorithm is compared with the classic multi-path fingerprint positioning and real-time monitoring method (SP algorithm) described previously. In the SP algorithm, a fingerprint database is established by dividing rectangular grids for positioning and the real-time monitoring areas, and the grid side lengths are set to  $int = 2m$  and  $1m$ , respectively. The positioning and real-time monitoring performance are evaluated by the root-mean square error (RMSE) and the cumulative distribution function (CDF) for the positioning and real-time monitoring error.

Table 1. Settings of system simulation parameters

Simulation Parameter	Parameter Value
Number of OFDM subcarriers	$K=16$
Number of ULA elements (M)	4/6/8/10/12
Signal bandwidth $B_w$ (MHz)	5/10/20
Number of samples collected for each snapshot in the SP algorithm	$N_s = 8$
Number of snapshots of the data points in the SP algorithm	$L_d = 50$
Number of snapshots of the test points in the SP algorithm	$L_t = 20$

Figure 6 shows the variation of the RMSE of the position estimation based on the two algorithms during the entire driving process of the vehicle. The results show that when the vehicle is far away from the RSU, the signal-to-noise ratio is reduced due to factors such as path loss and multi-path fading. The positioning and real-time monitoring performance of the two algorithms is relatively poor. It should be noted that the density of fingerprint data points of the database in the SP algorithm has a more significant impact on the positioning and real-time monitoring performance. When the number of data points increases, the positioning and real-time monitoring error of the SP algorithm is significantly reduced. However, given that the  $1\text{ m}$  grid side length in the fingerprint database is relatively dense already, although a denser grid may create higher accuracy, it can also lead to an exponential increase in computational complexity. From the figure, it can be seen that through the application of the WLS estimator, the proposed algorithm can significantly reduce the positioning and real-time monitoring errors in an environment with a low signal-to-noise ratio, with relatively good stability. In addition, it is superior to the SP algorithm in most cases. Figures 7 and 8 show the effect of the number of ULA array elements and the signal bandwidth on the CDF distribution of the positioning and real-time monitoring errors, respectively. It can be seen that with the increase of the antenna array elements and bandwidth, the spatial dimension and resolution of the signals have increased slightly. As a result, the positioning and real-time monitoring performance of the two algorithms have been improved. In particular, it can be observed from Figure 8 that when the number of ULA array elements is 8, and the signal bandwidth is 20 MHz, the error of about 98% of the vehicle position estimation based on the proposed algorithm is less than 2m. However, in the SP algorithm, the error of only 83.5% of the position estimation is less than 2m. From the results in the figure, it can be known that the performance of the proposed positioning and real-time monitoring

algorithm is superior to the multi-path fingerprint positioning and real-time monitoring method under different bandwidths and antenna array elements.

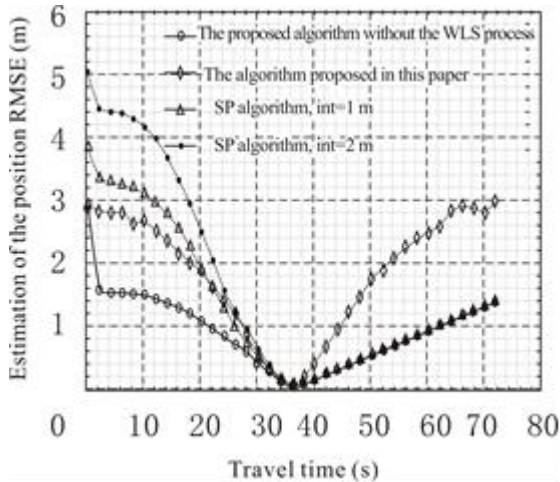


Figure 6. Comparison of the root mean square error between the proposed algorithm and the SP algorithm

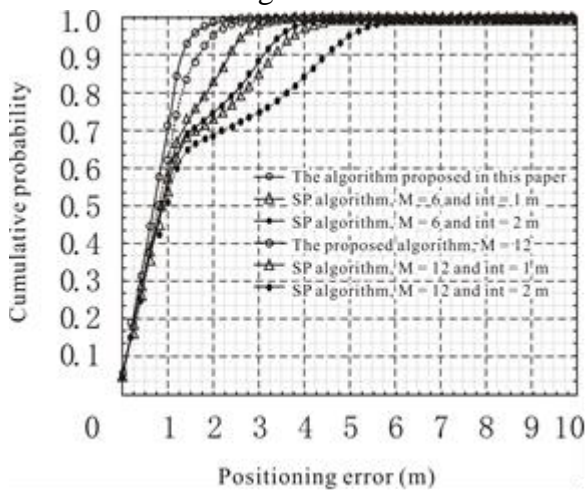


Figure 7. CDF distribution of the positioning and real-time monitoring errors of the proposed algorithm and the SP algorithm under different array elements ( $B_w = 10\text{MHz}$ )

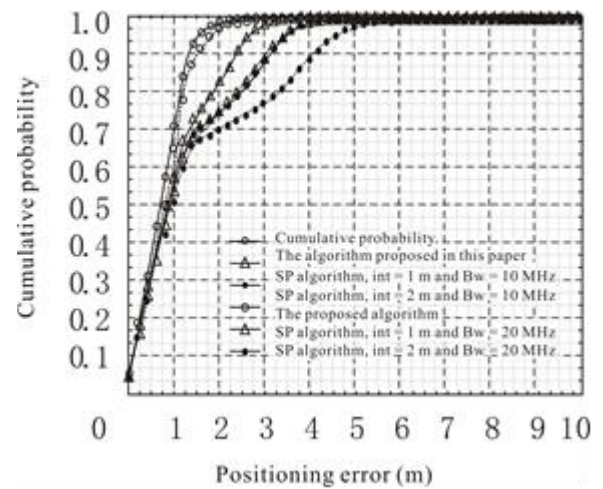


Figure 8. CDF distribution of the positioning and real-time monitoring errors of the proposed algorithm and the SP algorithm under different signal bandwidths ( $M = 8$ )

## 5. Conclusions

To solve the problems of precise real-time positioning and real-time monitoring of vehicles in the VANETs, we put forward the single station positioning and real-time monitoring algorithm of vehicles based on the RFID technology and the visual perception technology, respectively. In the positioning and real-time monitoring algorithm based on the RFID technology, the ULA array antenna is used at the vehicle end to carry out the positioning and real-time monitoring through the joint TOA/AOA estimation. In addition, the high-resolution estimation technology is introduced, and the frequency domain MP algorithm is used to process the received CFR matrix directly and obtain the real-time AOA estimation, thereby reducing the time overhead. Subsequently, the frequency diversity characteristics of OFDM subcarriers are further used to establish the model for the TOA high-resolution estimation as an NLF problem for the solution. The characteristics of the phase difference between adjacent subcarriers are used to correct the ill-conditioned state of the fitting function, which has improved the reliability of the results. Finally, the vehicle position is calculated by using the WLS estimator to implement high-precision real-time

positioning and real-time monitoring. The positioning and real-time monitoring algorithm based on visual perception is equipped with a visual sensor at the RSU end. Through the extraction of the image feature information within the perception range of the sensor, the target vehicle contour is obtained, and the corresponding centroid coordinates are calculated to complete the positioning and real-time monitoring. At the same time, the visual positioning and real-time monitoring results and the information of the inertial sensor with a relatively high sampling rate are used for integrated positioning and real-time monitoring through the UKF filter, which has further improved the accuracy of the positioning and real-time monitoring and the real-time performance of the algorithm. The simulation results suggest that, compared with the traditional multi-path fingerprint algorithm, the algorithm proposed in this paper has relatively good positioning and real-time monitoring performance even at a low signal-to-noise ratio (SNR).

## References

- [1] Hongqi, L. , Xinyu, C. , Wencong, Z. , & Yingrong, L.. (2016). The vehicle flow formulation and savings-based algorithm for the rollon-rolloff vehicle routing problem. *European Journal of Operational Research*, 257(3), 859-869.
- [2] Zhang, Y. , Gao, K. , Zhang, Y. , & Su, R.. (2019). Traffic light scheduling for pedestrian-vehicle mixed-flow networks. *IEEE Transactions on Intelligent Transportation Systems*, 20(4), 1468-1483.
- [3] Sun, Q. , Zhang, H. , & Mo, L.. (2011). Dual-reader wireless protocols for dense active rfid identification. *International Journal of Communication Systems*, 24(11), 1431-1444.
- [4] Chen, K. M. , Chen, J. C. , & Cox, R. A.. (2012). Real time facility performance monitoring system using rfid technology. *Assembly Automation*, 32(2), 85-196..
- [5] Sudhakar, S. , Chandankumar, A. , & Venkatakrishnan, L.. (2017). Influence of propeller slipstream on vortex flow field over a typical micro air vehicle. *The Aeronautical Journal*, 121(1235), 95-113.
- [6] Wang, J. , Gao, G. , Li, X. , Liang, X. , & Zhang, J.. (2019). Effect of bogie fairings on the flow behaviours and aerodynamic performance of a high-speed train. *Vehicle System Dynamics*(6), 1-21.
- [7] Song, X. , Li, X. , Tang, W. , & Zhang, W.. (2016). A fusion strategy for reliable vehicle positioning utilizing rfid and in-vehicle sensors. *Information Fusion*, 31, 76-86.
- [8] Herrojo, C. , Mata-Contreras, J. , Paredes, F. , & Ferran Martín. (2017). Microwave encoders for chipless rfid and angular velocity sensors based on s-shaped split ring resonators. *Sensors Journal IEEE*, 17(15), 4805-4813.
- [9] Torrisi, N. M. , & Oliveira, J. F. G. D.. (2012). Remote monitoring for high-speed cnc processes over public ip networks using cyberopc. *The International Journal of Advanced Manufacturing Technology*, 60(1-4), 191-200.
- [10] Amendola, S. , Bovesecchi, G. , Palombi, A. , Coppa, P. , & Marrocco, G.. (2016). Design, calibration and experimentation of an epidermal rfid sensor for remote temperature monitoring. *IEEE Sensors Journal*, 16(19), 7250-7257.